Asian Journal of Pharmaceutical Sciences 15 (2020) 482–491

Available online at www.sciencedirect.com

ScienceDirect

journal homepage: www.elsevier.com/locate/AJPS

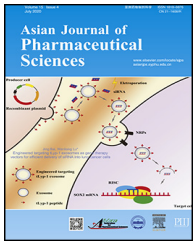

Original Research Paper

# *In situ* apolipoprotein E-enriched corona guides dihydroartemisinin-decorating nanoparticles towards LDLr-mediated tumor-homing chemotherapy

*Zhenbao Li*[a,b,c,1], *Jiaojiao Zhu*[a,1], *Yongqi Wang*[a], *Mei Zhou*[a], *Dan Li*[c], *Shunzhe Zheng*[c], *LiLi Yin*[d], *Cong Luo*[c], *Huicong Zhang*[c], *Lu Zhong*[c], *Wei Li*[e], *Jian Wang*[e], *Shuangying Gui*[a,b,**], *Biao Cai*[f,**], *Yongjun Wang*[c], *Jin Sun*[c,*]

[a] *College of Pharmacy, Anhui University of Chinese Medicine and Anhui Academy of Chinese Medicine, Hefei 230012, China*
[b] *Engineering Technology Research Center of Modernized Pharmaceutics, Education Office of Anhui Province, Hefei 230012, China*
[c] *Wuya College of Innovation, Shenyang Pharmaceutical University, Shenyang 110016, China*
[d] *Shenyang Heshi Pharmaceutical Co., Ltd., Shenyang 110163, China*
[e] *Key Laboratory of Structure-Based Drug Design and Discovery of Ministry of Education, Shenyang Pharmaceutical University, China*
[f] *School of Integrated Chinese and Western Medicine, Anhui University of Chinese Medicine, Hefei 230012, China*

ARTICLE INFO

*Article history:*
Received 30 January 2019
Revised 25 March 2019
Accepted 7 May 2019
Available online 5 July 2019

*Keywords:*
In situ ApoE-enriched corona
DHA decoration
Nanoparticulate drug delivery system
LDLr-mediated tumor-homing chemotherapy

ABSTRACT

The therapeutic efficiency of active targeting nanoparticulate drug delivery systems (nano-DDS) is highly compromised by the plasma proteins adsorption on nanoparticles (NPs) surface, which significantly hinders cell membrane receptors to recognize the designed ligands, and provokes the off-target toxicity and rapid clearance of NPs *in vivo*. Herein, we report a novel dihydroartemisinin (DHA)-decorating nano-DDS that *in situ* specifically recruits endogenous apolipoprotein E (apoE) on the NPs surface. The apoE-anchored corona is able to prolong PLGA-PEG2000-DHA (PPD) NPs circulation capability in blood, facilitate NPs accumulating in tumor cells by the passive enhanced permeability and retention (EPR) effect and low-density lipoprotein receptor (LDLr)-mediated target transport, and ultimately improve the *in vivo* antitumor activity. Our findings demonstrate that the strategy of *in situ* regulated apoE-enriched corona ensures NPs an efficient LDLr-mediated tumor-homing chemotherapy.



* Corresponding authors. Shenyang Pharmaceutical University, Shenyang 110016, China. Tel: +86 24 23986325.
** Corresponding authors. Anhui University of Chinese Medicine, Hefei 230012, China.
*E-mail addresses:* guishy0520@ahtcm.edu.cn (S.Y. Gui), caibiao9035@163.com (B. Cai), sunjin66@21cn.com (J. Sun).
[1] These authors contribute equally to this work.
Peer review under responsibility of Shenyang Pharmaceutical University.

https://doi.org/10.1016/j.ajps.2019.05.002

## 1. Introduction

Active targeting nanoparticulate drug delivery systems (nano-DDS) have been widely exploited as drug cargos for chemotherapy [1]. Among them, various strategies have been developed to functionalize nanoparticles (NPs) with biological ligands, aiming to specifically target to tumor cell receptors [2,3]. Though the ligand-functionalized strategy is effective *in vitro*, however, the corresponding *in vivo* targeting efficiency is significantly lessened or even diminished because NPs surface is nonspecifically opsonized by plasma proteins upon intravenous administration [3–5]. The formed protein corona mainly consists of high-affinity proteins such as complement components and immunoglobins [6–8], which induces undesired organ distribution and the quick clearance of NPs from the body [5,9–11]. Hydrophilic "stealth" polyethylene glycol (PEG) is supposed to prevent NPs from fouling of protein opsonins and extend NPs blood circulation time *in vivo* [12,13], nevertheless, the PEG-modification covers the targeting ligands and restrains the ligands to interact with membrane receptors [14,15], and also triggers the unsatisfied accelerated blood clearance (ABC) after repeated systemic administration [16].

Dihydroartemisinin (DHA), a metabolite of artemisinin, is efficient in antimalarial therapy [17]. *In vitro*, DHA exhibited a certain affinity to albumin or transferrin in an entropy-driven manner when incubation DHA with albumin or transferrin [18,19]. Therefore, we decorated DHA on the surfaces of PLGA-PEG2000-DHA (PPD) NPs and envisioned to prepare albumin or transferrin-enriched corona NPs. Differing from our assumption, we interestingly found that DHA-modified NPs could specifically recruit apolipoprotein (apoE), instead of albumin and transferrin, in their corona evidenced by LC-MS/MS and western blotting, taking bare PLGA-PEG2000 (PP) NPs as a control.

ApoE, an endogenous lipid-based transporting protein (40–70 μg/ml) [20], has been known to interact with the low-density lipoprotein receptor superfamily, such as low-density lipoprotein receptor (LDLr) and LDL receptor-related protein 1 receptor (LRP1r) [21,22]. Furthermore, the expression of LDLr and LRP1r is highly expressed on cancer cells [23]. Herein, we hypothesized that the *in situ* immobilized apoE-rich corona might salvage PPD NPs from reticuloendothelial system (RES) elimination, and promote NPs distributing into tumor cells by LDLr-mediated active targeting transport, both of which contribute to the enhanced anticancer activity *in vivo* (Fig. 1).

To validate this hypothesis, we synthesized the novel PPD conjugate by coupling DHA to terminal carboxyl of PLGA-PEG2000-COOH *via* a single ester bond linkage, and formulated PPD NPs via the emulsion solvent evaporation method. Then the next performances of apoE-recruited PPD NPs, such as pharmaceutical characterization, cell biological behaviors, pharmacokinetic, tissue distribution and the *in vivo* antitumor activity, were investigated as well.

## 2. Methods and materials

### 2.1. Materials

Docetaxel (DTX) is provided by Dalian Meilun Biotech Co., Ltd (Dalian, China). PLGA (50:50, Mw 8000)-PEG2000 was bought from Daigang Biomaterial Co., Ltd (Jinan, China). The Cy7-labeled polycaprolactone (Cy7-PCL) was obtained from

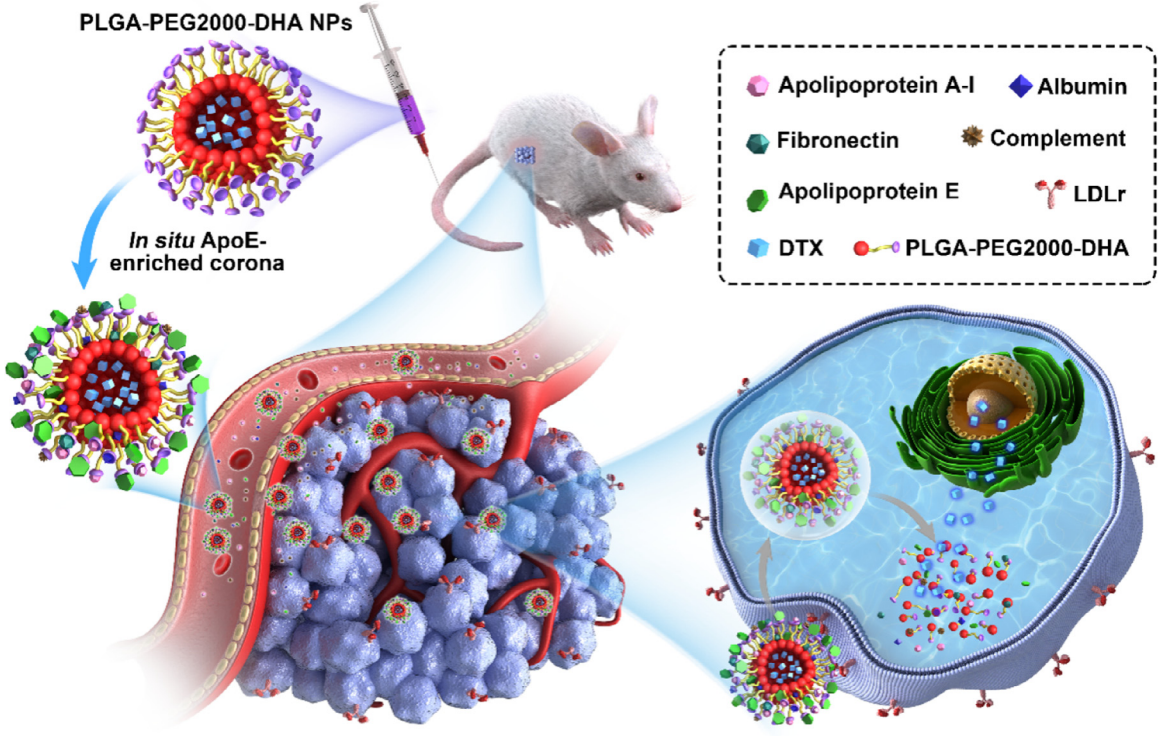


**Fig. 1 – Illustration of the *in situ* enriched apolipoprotein E corona ensure NPs LDLr-mediated tumor-homing chemotherapy.**

Shanghai Jinpan Biotech Co., Ltd (Shanghai, China). Anti-LDL receptor (ab52818), anti-Apolipoprotein E (ab183596) and anti-LRP1 antibody (ab92544) were purchased from abcam (London, UK). PLGA-PEG2000-DHA was synthesized in our lab. Solvents were all of the HPLC grade. All animals were tested in line with guidelines of the ethics committee of Anhui University of Chinese Medicine and Shenyang pharmaceutical university.

### 2.2. Synthesis of PPD

*Synthesis of PLGA-PEG2000-COOH:* PLGA-PEG2000-COOH was synthesized by ring-opening polymerization of lactide and glycolide, initiating by HO-PEG2000-COOH under the catalysis of stannous octoate [24]. In Brief, stannous octoate, glycolide and lactide, were mixed and stirred for 10 h at 140 °C under nitrogen. After the reaction, the product was dissolved with dichloromethane, precipitated in ice-cold diethyl ether and vacuum drying. The chemical structure of PLGA-PEG2000-COOH was confirmed by nuclear magnetic resonance (NMR).

*Synthesis of PPD:* PLGA-PEG2000-COOH, DHA (40-fold excess), EDCI and HOBT were dissolved with dichloromethane and stirred in ice-bath for 1 h. Then, the mixed solution was reacted at 37 °C for 48 h under nitrogen. After the reaction, the objective product was precipitated with ice-cold diethyl ether, purified by silica column chromatography.

### 2.3. Preparation and characterization of PPD NPs

PPD (20 mg) and DTX (1 mg) were dissolved in 1 ml dichloromethane, and then poured into 0.5% PVA solution (5 ml). The mixture was ultrasound at 300 W for 5 min. The emulsion was stirred overnight to remove the organic solvent, and then centrifuged to obtain PPD NPs. In order to study the *in vitro* cell uptake, coumarin-6 labeled PPD NPs (coumarin-6-PPD NPs) were prepared by the same method except for the substitution of DTX with coumarin-6. Meanwhile, Cy7 labeled PPD NPs (Cy7-PPD NPs) were prepared similarly except for the addition of Cy7-PCL (at 10% of matrix composition) to evaluate NPs *in vivo* distribution. PLGA-PEG2000 NPs (PP NPs) were formulated using the same method except PLGA-PEG2000 instead of PPD.

Size and zeta potential of PP NPs and PPD NPs were determined by Zetasizer (Nano ZS, Malvern, Co., U.K.). The morphology of these NPs was observed by transmission electron microscopy (TEM) (cryo-TEM, Hitachi, Japan).

### 2.4. Drug loading content (DL) and encapsulation efficiency (EE)

DL and EE were measured by centrifugation method. Unloaded DTX of PP NPs and PPD NPs was removed by centrifugation at rate of 3500 rpm for 30 min. Then, entrapped DTX was dissolved using acetonitrile and determined by HPLC method [25]. The corresponding DL and EE were calculated as follow:

$$DL(\%) = \frac{\text{amount of drug encapsulated in nanoparticles}}{\text{total amount of the nanoparticles}} \times 100\%$$

$$EE(\%) = \frac{\text{amount of drug encapsulated in nanoparticles}}{\text{total amount of drug added}} \times 100\%$$

### 2.5. Colloidal stability

Colloidal stability of PP NPs and PPD NPs were measured in PBS (pH 7.4) containing 10% of fetal bovine serum (FBS) by recording the diameter changes at 37 °C for 72 h. In order to explore long-term stability of PP NPs and PPD NPs, size was measured for one month at 4 °C.

### 2.6. Differential scanning calorimetry (DSC) and X-ray diffractometry (XRD)

DSC profiles of five samples: DTX, blank PP NPs, physical mixture of blank PP NPs and DTX, PP NPs and PPD NPs were measured by DSC-60 (Mettler-ToledoInternational Inc., Switzerland). Solid phase of DTX in the above five samples was characterized by XRD.

### 2.7. In vitro drug release

DTX release of PP NPs and PPD NPs were estimated by dialysis method. The NPs formulation (300 μg DTX equivalent) was sealed in a dialysis bag (Mw, 14 000) and immersed in 30 ml of pH 7.4 PBS supplemented with 1% tween 80 at 37 °C. The release of DTX was detected by the above established HPLC method.

### 2.8. Quantification of protein corona

Protein corona was isolated from NPs by centrifugation after incubation with rat serum for 1 h [25,26]. Taking PPD NPs as an example, incubated PPD NPs were washed by the repeated centrifugation (16 000 g for 10 min) and resuspension process with PBS to isolate weak-adsorbed soft corona. After five repeated washes, the following hard-adsorbed protein corona were completely removed by repeated centrifugation and suspension with pH 7.4 PBS buffer (containing 6% SDS solution) twice as above. The adsorbent proteins were the combination of the aforementioned soft-adsorbed and hard-adsorbed proteins, and then determined by liquid chromatography-mass spectrometry (LC-MS). The corresponding normalized spectral count (NpSpC) was calculated as follow:

$$\text{NpSpCk}(\%) = \frac{(\text{SpC}/\text{Mw})\text{k}}{\sum_{\text{i}=1}^{n}(\text{SpC}/\text{Mw})\text{i}} \times 100\%$$

where $\text{NpSpC}_\text{k}$ is the standardized percentage of the SpC for protein k and $\text{M}_\text{w}$ is the molecular weight of protein k. Meanwhile, the adsorbed proteins were also exploited to evaluate apoE adsorption by western blotting.

### 2.9. LDL and LRP1 receptor expression

Mouse breast cancer 4T1 cells (4T1) and fibroblasts NIH 3T3 cells (3T3) were cultured at 37 °C, in MEM/F12 medium or RPMI-1640 medium with 10% FBS. To achieve the LDLr-overexpressed 4T1 cells (4T1-G), 4T1 cells were in RPMI-1640 medium supplemented with 2% ultroser G medium, instead of 10% FBS, for 72 h before experiments [27,28]. The determination of LDLr and LPR1r was performed by enzyme-

linked immunoabsorbent assay (ELISA) kit as our previous report [25]. To further validate the selectivity of PPD NPs to cancerous and normal cells, we also measured the LDLr expression level on 3T3 cells. To observe the LDLr expression visually, 4T1 cells were plated at a density of $8 \times 10^4$ cells/ml in 24-well plates for 24 h, fixed with 4% paraformaldehyde, blocked with 1% bovine serum albumin and then incubated with primary antibody overnight at 4 °C. Alexa Fluor 488 conjugated anti-rabbit IgG was used as a secondary antibody. The nucleus was labeled with DAPI. Then, the cells were observed by confocal laser scanning microscopy (C2SI, Nikon, Japan). The corresponding LDLr expression of 4T1-G and 3T3 cells was also evaluated as the above performances. Moreover, the LDLr expression of 4T1, 4T1-G and 3T3 cells was evidenced by western blotting as well.

### 2.10. *Cytotoxicity assay and cellular uptake*

The cytotoxicity and cellular uptake were performed as our previous report [25]. 4T1 and 3T3 cells were seeded in 96-well plate at a density of $1.5 \times 10^4$ cells/ml and cultured for 24 h, respectively. After further incubation with DTX-Sol, PP NPs and PPD NPs at a series of concentrations for 48 h, the cells were incubated with 20 μl (5 mg/ml) MTT for 4 h and the corresponding absorbance of samples was measured at 490 nm. Cellular uptake was assessed on 4T1, 4T1-G and 3T3 cells with coumarin-6 solution, coumarin-6-PP NPs and coumarin-6-PPD NPs (500 ng/ml) at 37 °C for 2 h. Subsequently, the cells were washed, counterstained by DAPI and observed by confocal laser scanning microscopy. For quantitative analysis, the cells were harvested in PBS and analyzed by flow cytometer (FACSCalibur, BD Biosciences). In order to study the blocking performance, we added low density lipoprotein (LDL) into the media to block the LDLr uptake pathway.

4T1 cells were employed to investigate the endocytotic mechanisms of PPD NPs [25]. 4T1 cells were seeded in 12-well plates with 1 mL of media at a density of $8 \times 10^4$ cells/well for 24 h. Next, the cells were pre-incubated with different inhibitors, including sodium azide (6 μg/ml), chlorpromazine (5 μg/ml), quercetin (6 μg/ml), indomethacin (3 μg/ml), colchicine (8 μg/ml) and 30 μg/ml LDL for 1 h. Then, the medium was displaced by 500 ng/ml coumarin-6-PPD NPs containing the above inhibitors in serum-supplemented medium for another 2 h at 37 °C.

### 2.11. *Pharmacokinetics*

The pharmacokinetics of PP NPs and PPD NPs were studies on Sprague-Dawley rats at an equal DTX dose of 5 mg/kg. All rats were randomly divided into two groups, and the DTX concentration in plasma was measured by UPLC-MS/MS method [29].

### 2.12. *Biodistribution*

The *in vivo* distribution of PPD NPs and PP NPs were evaluated by the 4T1 tumor-bearing Balb/c mice. When the tumors were up to 300 $mm^3$, the mice were randomly divided into two groups. Cy7-labeled PP NPs and PPD NPs were intravenously administrated at an equivalent dose of 2 mg/kg Cy7. Then, the mice were sacrificed at 4 h and 24 h, and the major organs and tumors were imaged under caliper IVIS (PerkinElmer, USA). As such, the tumors were stained with LDLr primary antibody overnight at 4 °C and Alexa Fluor 488 conjugated anti-rabbit IgG secondary antibody, DAPI and then visualized with CLSM [30].

### 2.13. *In vivo anticancer effects [25]*

4T1 tumor-bearing mice were randomly divided into 4 groups (5 mice in each group) after the tumor size was 150 −200 $mm^3$. The mice were then intravenously injected with saline, DTX-Sol, PP NPs and PPD NPs at a dose of 10 mg/kg and at a 3-d interval (day 0, 3, 6 and 9). Body weight and tumor volume were measured every second day. To evaluate the safety of NPs formulations, Aspartate transaminase (AST), alanine transaminase (ALT), blood urea nitrogen (BUN) and creatinine, and the organ indexes were all determinated. Tumor cell apoptosis was imaged using apoptosis detection kit (Yeasen, china). The pathological change of the main organs were also observed by hematoxylin and eosin (H&E) staining.

### 2.14. *Statistical analysis*

All results were expressed as mean or mean ± SD (standard deviation). A one-way ANOVA was applied to test the significance in the experiments.

## 3. Results and discussion

### 3.1. *Synthesis and characterization of PPD*

PLGA-PEG2000-COOH was synthesized *via* melt-polymerization of lactide and glycolide [31]. Then, the novel apoE-recruiting conjugate PPD was obtained by coupling DHA to terminal carboxyl of PLGA-PEG200-COOH using a single ester bond linkage (Fig. S1). Successful synthesis of PLGA-PEG2000-COOH and PPD were validated by $^1$H NMR (Fig. S2).

### 3.2. *Characterization of PPD NPs*

DTX-loaded PP NPs and PPD NPs were formulated by the emulsion solvent evaporation method. As shown in Fig. 2A-2B and Table S1, PP NPs and PPD NPs were both uniform spherical structure, with size of about 145 nm and zeta potential of around −4 mV. The drug loading and encapsulated efficiency of PPD NPs were about 4.4% and 93%, which were comparable to these of PP NPs. DSC and XRD diagrams (Fig. S3) suggested the amorphous state of DTX trapping in both PPD NPs and PP NPs. Moreover, the PP NPs and PPD NPs exhibited favorable size stability ether in pH 7.4 PBS supplemented with 10% FBS at 37 °C for 72 h or in an extended period of time (1 month) at 4 °C (Fig. 2C-2D). Compared with our previous *in vitro* study of DTX-loaded PLGA (50:50, Mw 8000) NPs [25], these NP formulations showed a better sustained release performance owing to the existence of PEG shell, and DTX release percentage reached approximately 60% at 72 h (Fig. 2E).

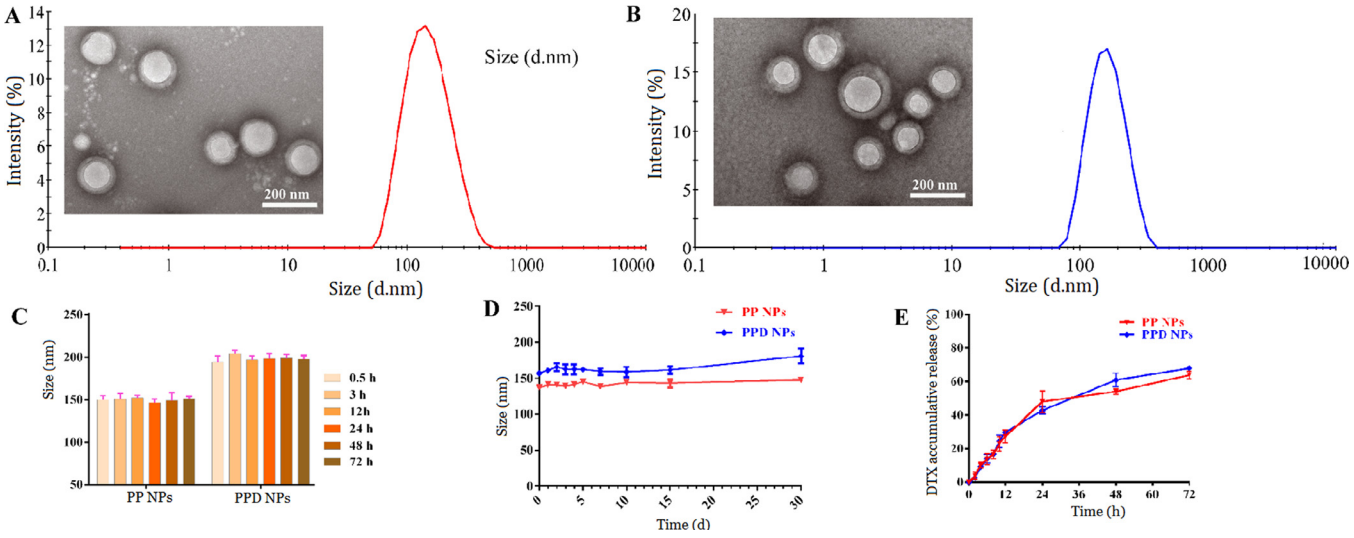


**Fig. 2 – Characterization of PPD NPs. TEM and size of (A) PP NPs and (B) PPD NPs. Size changes of NPs in (C) pH 7.4 PBS containing 10% FBS and (D) pH 7.4 PBS. (E) DTX release *in vitro*.**

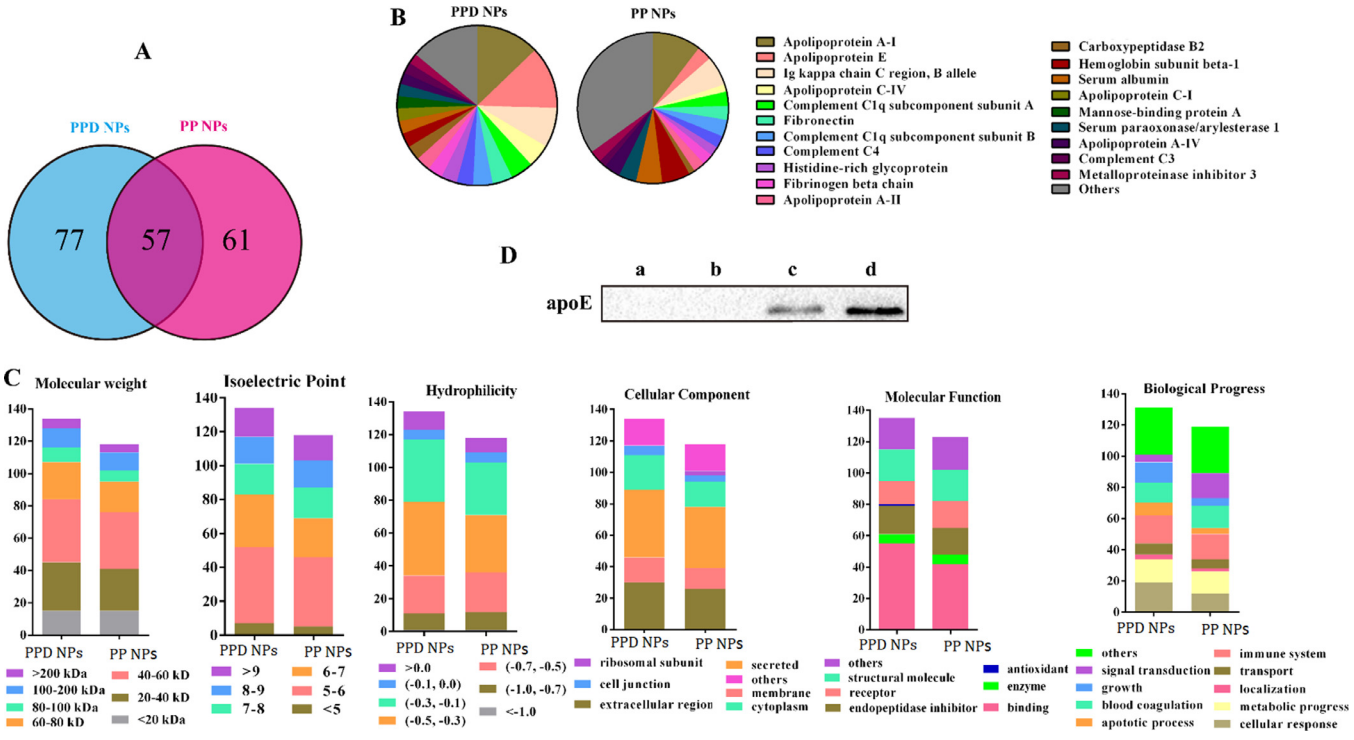


**Fig. 3 – Protein corona characterization. (A) Venn analysis of corona proteins types on PPD NPs and PP NPs. (B) The 20 Most-abundant corona proteins and proportion charts on PPD NPs and PP NPs. (C) Architectural cluster rank based on ontology. (D) Western blotting image of the adsorbed apoE after incubation of (c) PP NPs and (d) PPD NPs with rat serum for 1 h. The control samples were (a) PP NPs and (b) PPD NPs without rat serum incubation according to the same preparation process.**

### 3.3. *Corona protein analysis*

ApoE, an endogenous lipid transportion protein, is reported to bind the low-density lipoprotein receptor superfamily, such as LDLr and LRP1r [23]. Currently, apoE-based nano-DDS was mainly concentrated on brain-related investigation by precoating native apoE or tween 80 on the NPs surface before intravenous injection [23,32,33]. Unfortunately, the apoE-precoating strategy is immunogenic and expensive, and still unable to effectively evade the uncontrollable plasma opsonization, and also evokes the following off-target distribution and nanotoxicity to a certain degree [34,35]. Tween 80-coated NPs are reported to preferentially adsorb serum apoE to NPs surface after injection [36], but the

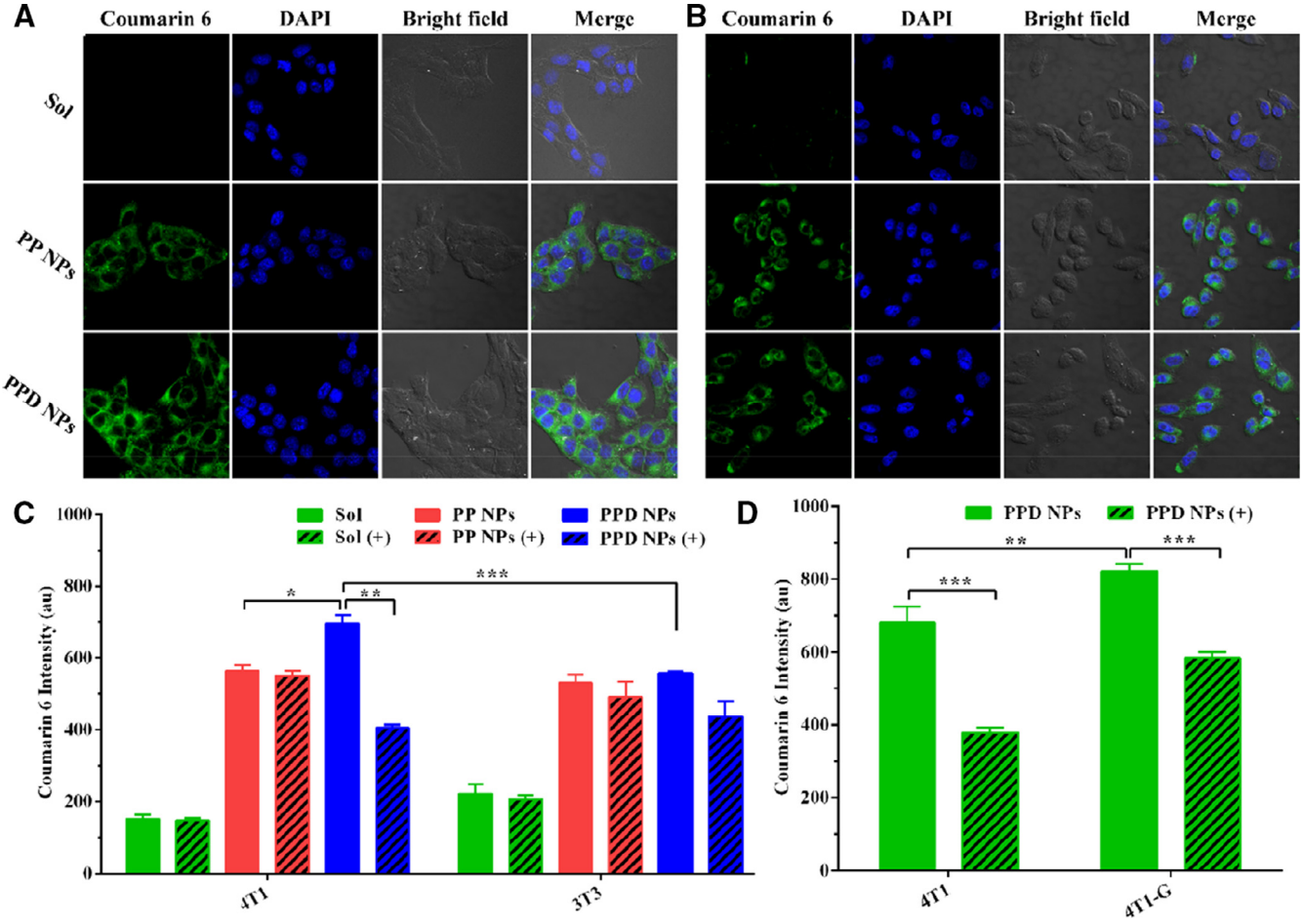


**Fig. 4 – Cellular uptake of the NPs in 4T1 and 3T3 cells. Fluorescence photographs of (A) 4T1 and (B) 3T3 cells incubated with NPs. Flow cytometry determination of NPs in (C) 4T1 and 3T3 cells with (+) or without LDL ($n = 3$). (D) Quantitative uptake efficiency of PPD NPs in 4T1 and 4T1-G cells with (+) or without LDL ($n = 3$). Data are expressed as the means ± SD, *$P < 0.05$, **$P < 0.01$ and ***$P < 0.001$.**

physically absorbed tween 80 possess potential hemolytic and allergic activity, and is also easily desorbed *in vivo* [37,38]. In this study, we first incubated NPs with rat serum at 37 °C for 1 h, isolated the adsorbed proteins by centrifugation and then determined the protein composition on NPs [26]. As illustrated in Fig. 3A, PPD NPs and PP NPs (as control in our study) adsorbed 134 and 118 kinds of proteins, respectively, 57 of which existed in both NP coronas components. We then ranked the 20 most abundant proteins of NPs corona (Table 1 and Fig. 3B), and discovered that the types and abundance of the adsorbed proteins in PPD NPs corona were different from that of PP NPs corona, which might confer NPs a different biological identity (Fig. 3C). To our surprise, we found that PPD NPs selectively recruited apoE from blood serum instead of transferrin or albumin (Fig. 3B and Table S2), and the apoE content on PPD NPs (~12.7%) was 4-fold higher than that on PP NPs (~3.2%). The interesting apoE-enriched corona might result from the combined contribution of size, zeta, shape, NPs surface feature and the complex biological milieu. Likewise, the preferentially anchored apoE on PPD NPs surfaces was also evidenced by western blotting (Fig. 3D), agreeing well with the above LC-MS/MS results.

### 3.4. *LDLr expression*

ApoE has been known to bind low-density lipoprotein receptor superfamily (*e.g.* LDLr and LRP1r) that facilitates the uptake of apoE or apoE-modified NPs, and the expression of LDLr and LRP1r is of high dependence on the cell lines [22,23]. Therefore, we employed ELISA kit to investigate the LDLr and LRP1r expression on cancerous 4T1 cells. As exhibited in Fig. S4A, the ELISA results revealed the LDLr amount (3.4 ng/mg) was 23-fold higher than LRP1r (0.14 ng/ml), which meant that LDLr is the main receptor on 4T1 cell for apoE-based NPs transport. Motivated by our previous study to differentiate carcinoma cells and normal cells, we next determine the LDLr expression on normal fibroblast 3T3 cells. As shown in Fig. S4B, 4T1 cells exhibited a 2.5-fold higher LDLr level than 3T3 cell, which was in good consistence with the result of western blotting and immunofluorescence (Fig. S5). Thus, the LDLr-overexpressed cancerous 4T1 cells and LDLr low-expressed normal 3T3 cells were selected to evaluate the differentiated potential of PPD NPs in the serum-containing medium.

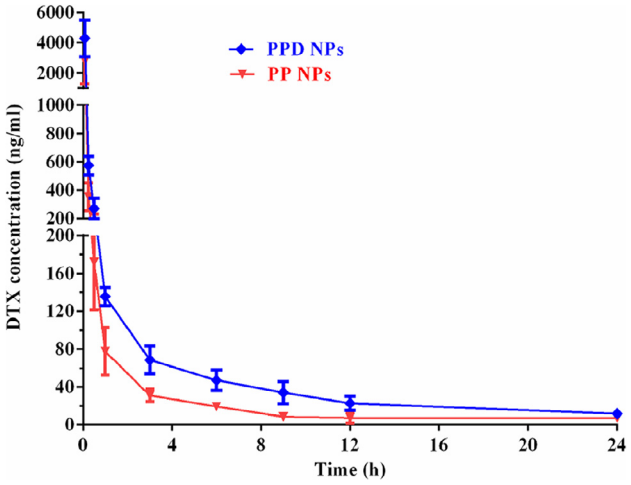


**Fig. 5 – Pharmacokinetic profiles of PPD NPs and PP NPs after intravenous injection of 5 mg/kg DTX. Data are showed as the means ± SD ($n = 4$).**

### 3.5. *Cytotoxicity and cellular uptake*

The cytotoxicity of PPD NPs and PP NPs was determined utilizing a MTT method. The cytotoxicity results of NPs on 4T1 and 3T3 cells both demonstrated a concentration-dependent mode. Comparing with DTX-Sol (solubilized by tween 80 and ethanol), both blank PP NPs and blank PPD NPs revealed little cytotoxicity (Fig. S6A-B). Among these formulations, DTX-Sol and PP NPs displayed a comparable cytotoxicity to 4T1 and 3T3 normal cells, whereas the growth inhibition of PPD NPs was about 3.1-fold greater in carcinoma 4T1 cells than in noncancerous 3T3 cells. This interesting performance indicated a high selectivity to tumor cells of PPD NPs in the serum-containing medium (Fig. S6C-6E and Table S3). Three main aspects were responsible for the increased cellular internalization. First, 4T1 cancer cells displayed a higher LDLr expression than 3T3 cells; next, LDLr favored the active uptake of the apoE-anchored PPD NPs into 4T1 cells in serum-supplemented medium; last, the enriched apoE-corona might be decomposed into amino acids to supply the excess growth of 4T1 cancer cells [39].

Next, we explored the cellular uptake of coumarin 6-labeled PPD NPs and PP NPs to 4T1 and 3T3 cells. The consequences in Fig. 4A-4C suggested PPD NPs had a greater internalization capability in 4T1 cells than in 3T3 cells, while the coumarin 6 Solution and coumarin 6-PP NPs demonstrated comparable internalization capacity to 4T1 and 3T3 cells, in good coincidence with the *in vitro* cytotoxicity consequences. Then, we added low density lipoprotein (LDL) into the media to block the LDLr of 4T1 cells before NPs addition. The addition of LDL significantly reduced the uptake efficiency of PPD NPs but had little influence on PP NPs internalization. To further testify the participation of LDLr in PPD NPs endocytosis, we used ultroser G to up-regulate the expression level of LDLr for 4T1 cells, named as "4T1-G". As shown in Fig. 4D, 4T1-G cells exhibited a higher internalization capability than 4T1 cells, and the enhanced uptake capacity could be inhibited by the addition of LDL as well.

Later, the internalization mechanism of PPD NPs into 4T1 cells was evaluated, where sodium azide/4 °C, chlorpromazine, quercetin, indomethacine, and colchicine were employed to inhibit the energy-involved, clathrin, clathrin/caveolin-independent, caveolin, and macropinocytosis manners, respectively. As delineated in Fig. S7, the cellular uptake of PPD NPs was involved in the aforementioned four pathways participation [40].

### 3.6. *Pharmacokinetics*

The impact of *in situ* immobilizing apoE-recruited corona on pharmacokinetic performance was studied by intravenous injection of PPD NPs and PP NPs into SD rats. As illustrated in Fig. 5 and Table S4, PP NPs demonstrated an extended circulation time (MRT∼6.2 h) owing to the PEG corona anti-fouling capability. In parallel, PPD NPs (MRT∼7.2 h) exhibited a comparable circulation efficiency and 1.9-fold improved AUC in comparison with the positive model PP NPs after the recruitment of apoE corona. This results indicated that the *in situ* formed apoE-rich corona could efficiently salvage PPD NPs from RES phagocytosis, which enables PPD NPs exerted a comparable circulation capacity to PP NPs.

### 3.7. *In vivo biodistribution*

The biodistribution of PPD NPs and PP NPs in 4T1 tumor-harboring mice was evaluated using caliper IVIS imaging. In comparison with PP NPs, PPD NPs presented a higher distribution in tumor mass, indicating that active targeting transport and passive EPR manner both participated in PPD NP delivery (Fig. 6A). Furthermore, it should be noticed that the *in situ* apoE-enrich corona also guided PPD NPs homing to the tumor cells *in vivo*, which might provide a hyper-selectivity to the LDLr-overexpressed tumor cells, as testified by the colocalized of LDLr-overexpressed 4T1 cell and Cy7-labeled PPD NPs (Fig. 6B). While apoE-based nano-DDS are main concentrated on brain diseases therapy, in our work, we found that PPD NPs were preferentially accumulated in subcutaneous tumor rather than brain tissue. From our perspective, three facets were supposed to the higher-distribution of PPD NPs in tumor. Firstly, 4T1 tumor tissue exhibited higher LDLr expression and a comparable LRP1r in comparison with brain tissue (Fig. S10). Next, active targeting and passive EPR effect were involved in PPD NP accumulation in tumor. Finally, blood-brain-barrier might significantly hinder PPD NPs (about 145 nm) trafficking into brain.

### 3.8. *In vivo antitumor activity*

4T1 tumor-harboring mice were employed to evaluate the *in vivo* anticancer capability of PPD NPs. Compared with the PBS and DTX-Sol groups, PP NPs exhibited a moderately delayed tumor growth performance (Fig. 7A–7C). By contrast, the mice injected with PPD NPs significantly lessened the volume of tumor, and the final tumor volume was about 200 $mm^3$ after the last treatment. Moreover, PPD NPs triggered significant tumor cell apoptosis in contrast with PBS, DTX-Sol and PP NPs (Fig. S8). Negligible changes in

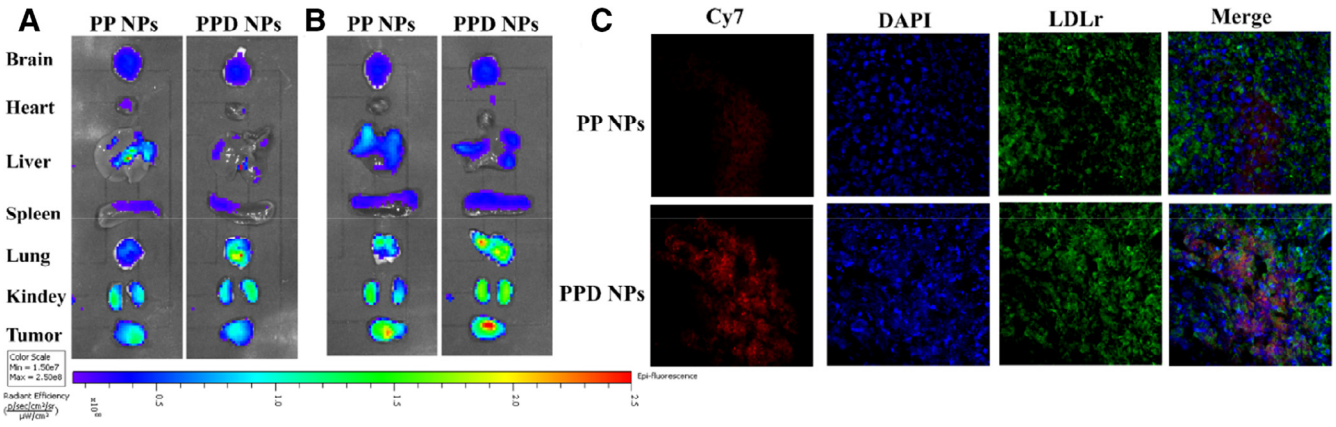


**Fig. 6 – *In vivo* fluorescence distribution of Cy7-labeled NPs at (A) 4 h and (B) 24 h. (C) Immunofluorescence of LDLr and Cy7-labeled PPD NPs. Overlap indicates the uptake of PPD NPs by 4T1 cells.**

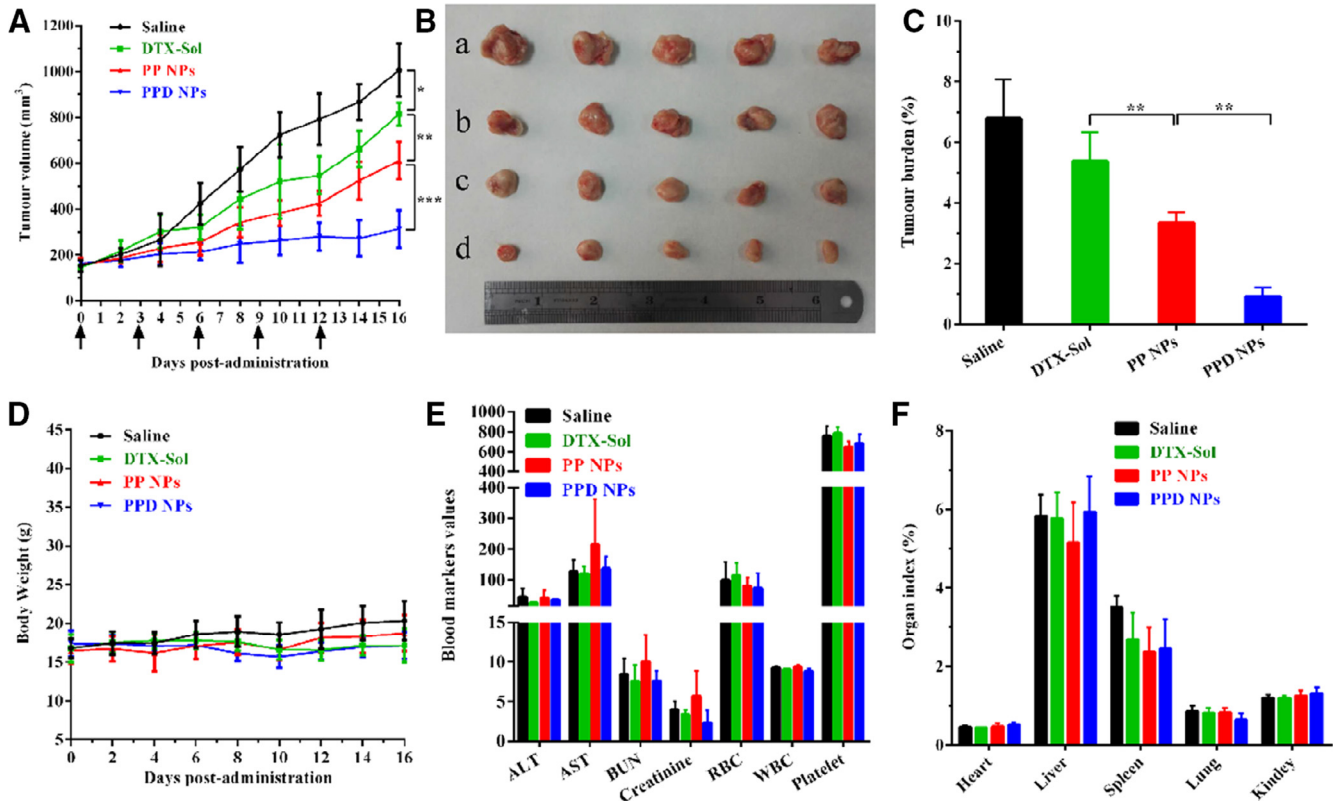


**Fig. 7 – *In vivo* anticancer activity of NPs. (A) 4T1 tumor growth profiles after the intravenous administration of diverse preparations ($n = 5$). (B) Image of tumors after the last treatment, where a–d were saline, DTX-Sol, PP NPs and PPD NPs, respectively. (C) Tumor burden calculating according to the weight of tumors divided by the average body weight of the mice ($n = 5$). (D) Body weight evolutions ($n = 5$), (E) hematological parameters ($n = 3$), (F) organ index ($n = 5$) of mice harboring 4T1 tumor xenografts after treatment. Data are the means ± SD, *$P < 0.05$ and **$P < 0.01$.**

the safety indicators, such as the body weight, organ index, hematological parameters and histological changes, were determined in mice after each group treatment (Fig. 7D–7E and Fig. S9). Several factors contribute to the potent antitumor activity and safety of this *in situ* immobilized apoE-enriched PPD NPs: (i) favorable colloidal stability owing to a steric PEG2000 shell protection; (ii) satisfied blood circulation *in vivo*; (iii) preferential distribution in the tumor by the passive EPR effect [30]; (iv) elevated cellular internalization in tumor cells due to the LDLr-mediated active transport and the ample nutritional need. All these above advantages contribute to the efficient chemotherapy and minimum off-target toxicities. Our investigations evidenced that the *in situ* strategy, on the basis of regulation of apoE-enriched corona, is highly potential to LDLr-based tumor-homing chemotherapy.

## 4. Conclusions

In this study, we elegantly designed DHA-coating nano-DDS that *in situ* anchors endogenous apoE in its corona, and then the resultant apoE-riched corona guides PPD NPs to achieve tumor-targeting capability. Following intravenous injection, the *in situ* formed apoE-rich corona could salvage PPD NPs from RES elimination, facilitate NPs entering into the tumor cells via the passive EPR distribtion and LDLr-mediated active targeting transport, and eventually endow PPD satisfied *in vivo* antitumor activity. Our study demonstrates that the strategy, based on the selective regulation of serum protein corona *in situ*, paves a potential avenue for the novel tumor-targeting nano-DDS design.

## Conflict of interest

The authors declare that there is no conflicts of interest.

## Acknowledgments

This work was supported by Anhui University of Chinese Medicine Foundation (No. 2019zrzd13), the Key Project of Anhui Province Department of Education (No. KJ2019A0471), the Key Project of Liaoning Province Department of Education (No. 2017LZD03), the National Nature Science Foundation of China (Nos. 81473164, 81703451, 81873019 and 81873351, U1608283).

## Supplementary material

Supplementary material associated with this article can be found, in the online version, at doi:10.1016/j.ajps.2019.05.002.

REFERENCES

[1] Li HJ, Du JZ, Du XJ, Xu CF, Sun CY, Wang HX, et al. Stimuli-responsive clustered nanoparticles for improved tumor penetration and therapeutic efficacy. Proc Natl Acad Sci USA 2016;113(15):4164–9.
[2] Kang T, Li F, Baik S, Shao W, Ling D, Hyeon T. Surface design of magnetic nanoparticles for stimuli-responsive cancer imaging and therapy. Biomaterials 2017;136:98–114.
[3] Salvati A, Pitek AS, Monopoli MP, Prapainop K, Bombelli FB, Hristov DR, et al. Transferrin-functionalized nanoparticles lose their targeting capabilities when a biomolecule corona adsorbs on the surface. Nat Nanotechnol 2013;8(2):137–43.
[4] Hadjidemetriou M, Al-Ahmady Z, Mazza M, Collins RF, Dawson K, Kostarelos K. *In vivo* biomolecule corona around blood-circulating, clinically used and antibody-targeted lipid bilayer nanoscale vesicles. ACS Nano 2015;9(8):8142–56.
[5] Kelly PM, Aberg C, Polo E, O'Connell A, Cookman J, Fallon J, et al. Mapping protein binding sites on the biomolecular corona of nanoparticles. Nat Nanotechnol 2015;10(5):472–9.
[6] Ke PC, Lin S. A decade of the protein corona. ACS Nano 2017;11(12):11773–6.
[7] Lundqvist M, Stigler J, Elia G, Lynch I, Cedervall T, Dawson KA. Nanoparticle size and surface properties determine the protein corona with possible implications for biological impacts. Proc Natl Acad Sci USA 2008;105(38):14265–70.
[8] Fleischer CC, Payne CK. Nanoparticle surface charge mediates the cellular receptors used by protein-nanoparticle complexes. J Phys Chem B 2012;116(30):8901–7.
[9] Meena AK, Ratnam DV, Chandraiah G, Ankola DD, Rao PR, Kumar MN. Oral nanoparticulate atorvastatin calcium is more efficient and safe in comparison to Lipicure in treating hyperlipidemia. Lipids 2008;43(3):231–41.
[10] Schottler S, Becker G, Winzen S, Steinbach T, Mohr K, Landfester K, et al. Protein adsorption is required for stealth effect of poly(ethylene glycol)- and poly(phosphoester)-coated nanocarriers. Nat Nanotechnol 2016;11(4):372–7.
[11] Walkey CD, Chan WC. Understanding and controlling the interaction of nanomaterials with proteins in a physiological environment. Chem Soc Rev 2012;41(7):2780–99.
[12] Nakamura M, Hayashi K, Nakano M, Kanadani T, Miyamoto K, Kori T, et al. Identification of polyethylene glycol-resistant macrophages on stealth imaging *in vitro* using fluorescent organosilica nanoparticles. ACS Nano 2015;9(2):1058–71.
[13] Cruz LJ. The influence of PEG chain length and targeting moiety on antibody-mediated delivery of nanoparticle vaccines to human dendritic cells. Biomaterials 2011;32(28):6791–803.
[14] Han X, Li Z, Sun J, Luo C, Li L, Liu Y, et al. Stealth CD44-targeted hyaluronic acid supramolecular nanoassemblies for doxorubicin delivery: probing the effect of uncovalent pegylation degree on cellular uptake and blood long circulation. J Control Rel 2015;197:29–40.
[15] Su G, Jiang H, Xu B, Yu Y, Chen X. Effects of protein corona on active and passive targeting of cyclic RGD peptide-functionalized PEGylation nanoparticles. Mol Pharm 2018;15(11):5019–30.
[16] Simon J, Wolf T, Klein K, Landfester K, Mailander V, Wurm FR. Hydrophilicity regulates the stealth properties of polyphosphoester-coated nanocarriers. Angew Chem Int Ed Engl 2018;57(19):5548–53.
[17] Ma YN, Xu DB, Li L, Zhang F, Fu XQ, Shen Q, et al. Jasmonate promotes artemisinin biosynthesis by activating the TCP14-ORA complex in Artemisia Annua. Sci Adv 2018;4(11):eaas9357.
[18] Veerappan A, Eichhorn T, Zeino M, Efferth T, Schneider D. Differential interactions of the broad spectrum drugs artemisinin, dihydroartemisinin and artesunate with serum albumin. Phytomedicine 2013;20(11):969–74.
[19] Yang Y, Zhang X, Wang X, Zhao X, Ren T, Wang F, et al. Enhanced delivery of artemisinin and its analogues to cancer cells by their adducts with human serum transferrin. Int J Pharm 2014;467(1–2):113–22.
[20] Mahley RW, Weisgraber KH, Huang Y. Apolipoprotein E: structure determines function, from atherosclerosis to Alzheimer's disease to AIDS. J Lipid Res 2009;50:S183–8 Suppl.
[21] Chen YC, Pohl G, Wang TL, Morin PJ, Risberg B, Kristensen GB, et al. Apolipoprotein E is required for cell proliferation and survival in ovarian cancer. Cancer Res 2005;65(1):331–7.
[22] Leyva-Gomez G, Cortes H, Magana JJ, Leyva-Garcia N, Quintanar-Guerrero D, Floran B. Nanoparticle technology for treatment of Parkinson's disease: the role of surface phenomena in reaching the brain. Drug Discov Today 2015;20(7):824–37.
[23] Zheng G, Chen J, Li H, Glickson JD. Rerouting lipoprotein nanoparticles to selected alternate receptors for the targeted

delivery of cancer diagnostic and therapeutic agents. Proc Natl Acad Sci USA 2005;102(49):17757–62.
[24] Hosseininasab S, Pashaei-Asl R, Khandaghi AA, Nasrabadi HT, Nejati-Koshki K, Akbarzadeh A, et al. Synthesis, characterization, and *in vitro* studies of PLGA-PEG nanoparticles for oral insulin delivery. Chem Biol Drug Des 2014;84(3):307–15.
[25] Li Z, Li D, Li Q, Luo C, Li J, Kou L, et al. In situ low-immunogenic albumin-conjugating-corona guiding nanoparticles for tumor-targeting chemotherapy. Biomater Sci 2018;6(10):2681–93.
[26] Fleischer CC, Payne CK. Nanoparticle-cell interactions: molecular structure of the protein corona and cellular outcomes. Acc Chem Res 2014;47(8):2651–9.
[27] Luiza Andreazza N, Vevert-Bizet C, Bourg-Heckly G, Sureau F, Jose Salvador M, Bonneau S. Berberine as a photosensitizing agent for antitumoral photodynamic therapy: insights into its association to low density lipoproteins. Int J Pharm 2016;510(1):240–9.
[28] Huntosova V, Buzova D, Petrovajova D, Kasak P, Nadova Z, Jancura D, et al. Development of a new LDL-based transport system for hydrophobic/amphiphilic drug delivery to cancer cells. Int J Pharm 2012;436(1–2):463–71.
[29] Li Z, Shang L, Liu C, Ma P, Wu C, Zhang W, et al. Evaluation of pharmacokinetics underlies the collaborated usage of lamivudine and oxymatrine in beagle dogs. Asian J Pharm Sci 2016;11(5):641–7.
[30] Lin T, Zhao P, Jiang Y, Tang Y, Jin H, Pan Z, et al. Blood-brain-barrier-penetrating albumin nanoparticles for biomimetic drug delivery via albumin-binding protein pathways for antiglioma therapy. ACS Nano 2016;10(11):9999–10012.
[31] Hong W, Chen D, Jia L, Gu J, Hu H, Zhao X, et al. Thermo- and pH-responsive copolymers based on PLGA-PEG-PLGA and poly(L-histidine): synthesis and *in vitro* characterization of copolymer micelles. Acta Biomater 2014;10(3):1259–71.
[32] Zhao N, Liu CC, Qiao W, Bu G. Apolipoprotein E, receptors and modulation of Alzheimer's disease. Biol Psychiatry 2017;83(4):347–57.
[33] Thaxton CS, Rink JS, Naha PC, Cormode DP. Lipoproteins and lipoprotein mimetics for imaging and drug delivery. Adv Drug Deliv Rev 2016;106(Pt A):116–31.
[34] Magro RD, Albertini B, Beretta S, Rigolio R, Donzelli E, Chiorazzi A, et al. Artificial apolipoprotein corona enables nanoparticle brain targeting. Nanomedicine 2017;14(2):429–38.
[35] Schaffler M, Sousa F, Wenk A, Sitia L, Hirn S, Schleh C, et al. Blood protein coating of gold nanoparticles as potential tool for organ targeting. Biomaterials 2014;35(10):3455–66.
[36] Aggarwal P, Hall JB, McLeland CB, Dobrovolskaia MA, McNeil SE. Nanoparticle interaction with plasma proteins as it relates to particle biodistribution, biocompatibility and therapeutic efficacy. Adv Drug Deliv Rev 2009;61(6):428–37.
[37] Kaur G, Mehta SK. Developments of polysorbate (Tween) based microemulsions: preclinical drug delivery, toxicity and antimicrobial applications. Int J Pharm 2017;529(1–2):134–160.
[38] Khan AR, Liu M, Khan MW, Zhai G. Progress in brain targeting drug delivery system by nasal route. J Control Rel 2017;268:364–89.
[39] Kratz F. A clinical update of using albumin as a drug vehicle - a commentary. J Control Rel 2014;190:331–6.
[40] He YJ, Xing L, Cui PF, Zhang JL, Zhu Y, Qiao JB, et al. Transferrin-inspired vehicles based on pH-responsive coordination bond to combat multidrug-resistant breast cancer. Biomaterials 2017;113:266–78.